

## Temperature fronts and vortical structures in turbulent stably stratified atmospheric boundary layers

Peter P. Sullivan[1], Jeffrey C. Weil[1, 2], Edward G. Patton[1],  
Harmen J. J. Jonker[3], Dmitrii V. Mironov[4]

<sup>1</sup>National Center for Atmospheric Research, Boulder, CO

<sup>2</sup>CIRES, University of Colorado Boulder, Boulder, CO

<sup>3</sup>Department of Civil Engineering and Geosciences, Delft University of Technology, Netherlands

<sup>4</sup>German Weather Service, Offenbach am Main, Germany

### INTRODUCTION

The nighttime stable atmospheric boundary layer (SBL) is a canonical example of a geophysical stably stratified shear flow. Its turbulent dynamics can be highly variable or even globally intermittent depending on the steadiness of the external forcing, variations in the underlying land surface properties, terrain undulations, and level of stratification [1]. Intermittent SBL turbulence impacts climate and weather modeling, electromagnetic wave propagation, interpreting observations collected from towers and kites, and air quality. In the present work, the dynamics of the SBL are examined in a regime where the level of forcing and stratification maintain continuous turbulence, *i.e.*, the so-called weakly stable boundary layer with statistically stationary turbulence. As a result, large eddy simulation (LES) with conventional subgrid-scale (SGS) models can then be used to explore the dynamics and coherent structures of the weakly stable boundary layer provided there is wide separation between the large and small scales of motion, *i.e.*, fine grids [2].

### SIMULATIONS

The SBL flow examined here is the first GEWEX Atmospheric Boundary Layer Study (GABLS1 boundary layer) described in [3]. This high-latitude SBL is a benchmark intercomparison case for canonical stable LES. It is driven by steady geostrophic winds  $(U_g, V_g) = (8, 0) \text{ m s}^{-1}$ , but with time varying surface temperature that decreases at the rate  $C_r = 0.25 \text{ K hr}^{-1}$  and induces stable stratification. External inputs are the Coriolis parameter  $f = 1.39 \times 10^{-4} \text{ s}^{-1}$ , surface roughness  $z_o = 0.1 \text{ m}$  for momentum and temperature, buoyancy parameter  $\beta = 3.70 \times 10^{-2} \text{ m s}^{-2} \text{ K}^{-1}$ , and still air potential temperature  $\theta_o = 265 \text{ K}$ . For the GABLS1 set of inputs, multiple LES codes, including the present one, with different SGS models and numerics predict a well developed near equilibrium SBL is reached after 9 physical hours with stratified rotated winds featuring a low-level super-geostrophic wind maximum of about  $10 \text{ m s}^{-1}$  below the boundary layer top  $z_i \sim \mathcal{O}(150 - 200) \text{ m}$ . In the present work we consider stronger surface cooling rates  $C_r = [0.25, 0.375, 0.5, 1.0] \text{ K hr}^{-1}$ , referred to as simulations [S1, S2, S3, S4], respectively. The computational domain is  $(L_x, L_y, L_z) = (400, 400, 400) \text{ m}$  and the mesh is  $1024^3$  gridpoints - hence the resolution is extremely fine  $\Delta = 0.39 \text{ m}$  in all three coordinate directions. The simulations are integrated for 9 physical hours which requires approximately 900,000 time steps. For the range of cooling rates considered the bulk stable stratification  $z_i/L$  increases from 1.7 to nearly 6 ( $z_i$  is the SBL height and  $L$  is the Monin-Obukhov length). Bulk statistics obtained from the simulations are provided in Table 1.

### RESULTS

To provide background for our discussion of coherent structures in the SBL, we first present vertical profiles of mean winds  $\langle u, v \rangle$ , mean potential temperature  $\langle \theta \rangle$ , squared (buoyancy, shear) frequencies  $(N^2, S^2)$ , and gradient Richardson number  $Ri = N^2/S^2$  in Figs. 1 and 2. These profiles are obtained by averaging in  $x - y$  horizontal planes and over the last hour of the simulation. Under this heavy averaging all the profiles are smoothly varying functions of height. The impact of surface cooling is readily apparent. As  $C_r$  (or the bulk stratification) increases, the SBL is shallower, the height of the low-level jet (LLJ) descends, the winds turn more sharply with height, and the surface wind stress decreases. The mean temperature profile develops

Case	$C_r$ (K hr <sup>-1</sup> )	$z_i$ (m)	$u_*$ (m s <sup>-1</sup> )	$Q_* \times 10^3$ (K m s <sup>-1</sup> )	$\theta_*$ (K)	$L$ (m)	$z_i/L$	$z_j/z_i$
S1	0.25	197.5	0.255	-9.63	0.0378	116.4	1.70	0.796
S2	0.375	182.0	0.234	-11.53	0.0493	74.7	2.44	0.746
S3	0.5	172.8	0.222	-13.48	0.0607	54.7	3.16	0.706
S4	1.0	154.1	0.194	-19.47	0.1004	25.5	6.04	0.589

Table 1: Bulk simulation properties.  $C_r$  is the surface cooling rate;  $z_i$  is the SBL top; ( $u_*$ ,  $Q_*$ ,  $\theta_*$ ) are the surface friction velocity, kinematic temperature flux, and temperature scale;  $L$  is the Monin-Obukhov stability length;  $z_i/L$  is a measure of the bulk boundary layer stability, and  $z_j/z_i$  is the location of the wind low-level jet (LLJ) maximum relative to  $z_i$ .

sharper vertical gradients in the lower boundary layer, leading to an increase in the surface temperature flux, and the temperature gradients are weaker aloft especially so for simulation S4 with the highest cooling rate. The Richardson number varies smoothly with the highest value approaching the critical value  $Ri \sim 0.25$  at the location of the LLJ. In S4, the sharp increase and decrease in  $Ri$  near the LLJ occurs because of delicate transitions in the shear and buoyancy frequencies (left panel of Fig. 2). For all cooling rates resolved turbulence dominates as the ratio of the subgrid-scale energy  $\langle e \rangle$  to the total turbulence kinetic energy (TKE) is  $\leq 15\%$  even in the region above the LLJ. The grid spacing  $\Delta$  is less than the Ozmidov scale  $L_o = \sqrt{\langle \epsilon \rangle / \langle N^2 \rangle^{3/2}}$  over the entire domain;  $\epsilon = C_\epsilon e^{3/2} / \Delta$  with  $C_\epsilon \sim 0.93$  is the SGS dissipation model.

One of the most ubiquitous features in all simulations, over the stratification range  $z_i/L = [1.7, 6]$ , is the presence of temperature fronts that populate the SBL, see Fig. 3. The fronts mark a sharp boundary separating warm (upstream) and cool (downstream) air. Animations show that these sharp fronts are tilted in the downstream direction, exhibit spatial spanwise and vertical coherence and propagate in time as organized entities. We note scalar fronts are often observed in direct numerical simulations of homogeneous stratified shear flow with no boundaries [4,5], and in passive scalar turbulence [6].

In the SBL, the tilt of a temperature front varies with stratification. Decomposing the temperature into a horizontal mean and turbulent fluctuation and applying vector algebra shows that a constant  $\theta$ -surface has instantaneous tilt angles  $\phi_\perp = (\phi_1, \phi_2)$  in the  $(x, y)$  directions:

$$\tan \phi_1 \hat{\mathbf{x}} + \tan \phi_2 \hat{\mathbf{y}} = \frac{-1}{\partial \langle \theta \rangle / \partial z + \partial \theta' / \partial z} \left( \frac{\partial \theta'}{\partial x} \hat{\mathbf{x}} + \frac{\partial \theta'}{\partial y} \hat{\mathbf{y}} \right), \quad (1)$$

where  $\phi_\perp$  is taken positive counter-clockwise from a horizontal plane [2]. Based on (1) the tilt angle increases (decreases) depending on the magnitude of the background stratification relative to the turbulent temperature fluctuations. Evidently, the fronts in the lower panel of Fig. 3 are tilted more towards the  $x$ -axis because of the stronger mean stratification in simulation S4 compared to S1. Color contours of normalized temperature fluctuations  $\tilde{\theta}' = (\theta - \langle \theta \rangle) / \theta_*$  in  $x-y$  planes at a height  $z/z_i = 0.2$ , where continuous turbulence is maintained, are presented in Fig. 4. Numerous fronts are intermittently sprinkled throughout the horizontal domain. They are intense, for example a typical jump across a front can be  $\Delta \theta = (0.2, 0.6)$  degrees or more for simulations (S1, S4), respectively. A frontal boundary is also aligned perpendicular to the mean horizontal winds at this height; winds are rotated (30.6, 32) degrees from the horizontal  $x$ -axis for (S1, S4). The zoomed images in the lower panel of Fig. 4 provide a sense of the spatial variability and scale of the warm-cool regions. The number of fronts increases while their scale decreases with increasing stratification. Finally, we emphasize that these warm-cool temperature fronts are internally generated by the dynamical interaction between shear turbulence and a stably stratified temperature field since the surface boundary conditions and the external geostrophic pressure gradients in the LES are horizontally homogeneous.

What are the stratified turbulent dynamics and coherent structures that generate temperature fronts in the SBL? Can we quantify the average state of the turbulent flow near a temperature front? To investigate these questions we next perform event based conditional sampling. In the language of turbulent structure identification we are interested in the average state of the SBL flow fields subject to a particular set of

prescribed events  $E$ , that is near a front we wish to compute conditional averages  $\hat{f} = \langle f|E \rangle$  where  $\hat{f} = (\hat{\mathbf{u}}, \hat{p}, \hat{\theta})$ . We adopt the technique of linear stochastic estimation pioneered by Adrian [7] as the preferred method of computing  $\hat{f}$ . For our application, the detection rule is two events, positive (upstream) and negative (downstream) temperature perturbations  $E$ , separated by a distance  $d$  - essentially this serves as a simple model of the observed fronts in Fig. 4 where the temperature jump  $\Delta\theta \sim 2E$ . Conditional perturbation fields  $(\hat{\mathbf{u}}, \hat{p}, \hat{\theta})$  are found by varying two parameters the amplitude of the events and their spatial separation [2]. The conditional velocity gradient matrix  $\partial\hat{u}_i/\partial x_j$  and vorticity field  $\hat{\omega} = \nabla \times \hat{\mathbf{u}}$ , which can be used to identify vortical structures, are then easily computed by post-processing  $\hat{\mathbf{u}}$ .

Results for simulations S1 and S4 are provided in Figs. 5 and 6. In both cases, the normalized event amplitude  $2Eu_*/Q_* = 5.29$ , and the separation distance  $d$  is chosen to lie near the scale of the peak in the co-spectrum between  $u$  and  $\theta$ . Thus the event amplitude and scale are typical of turbulence in the energy containing range. Vortical structures are first identified by determining the complex part of the eigenvalues of the conditional velocity gradient matrix  $\partial\hat{u}_i/\partial x_j$ , *i.e.*, the so-called  $\lambda_{ci}$  method [2,8]. The results shown in Figs. 5 and 6 are intriguing. We find closely coupled vortical structures rotated so as to align with the mean wind direction upstream and downstream of a frontal boundary. Independent of the stratification, the vortices are tilted vertically at an angle near 45 degrees from the horizontal. It is interesting to note that this angle is steeper than observed in *unsteady* homogeneous shear flow [5] at late time. The downstream structure appears to be an upward pointing hairpin vortex with closely spaced legs while the upstream structure more nearly resembles a circular ring vortex. Because the vertical legs are closely spaced the connecting arch bridging the legs is less pronounced. The vortices induce vigorous quadrant 2 and 4 negative vertical momentum fluxes along with negative-vertical and positive-horizontal temperature fluxes. The main effect of stratification, for the range of  $z_i/L$  considered, is to reduce the scale of the vortical structures, but not their overall shape, as shown by a comparison of the flow patterns in Figs. 5 and 6. The vortical structures in the SBL with stratification up to  $z_i/L = 6$  appear to be cousins to their counterparts extensively studied in neutral smooth wall boundary layers [9].

*Acknowledgments:* This work is supported by the National Science Foundation through the National Center for Atmospheric Research (NCAR). This research benefited greatly from computer resources provided by the NCAR Strategic Capability Program and the Department of Defense High Performance Computing Modernization Program.

## References

- [1] L. Mahrt 2014, *Stably stratified atmospheric boundary layers*, Annual Review of Fluid Mechanics **46**, 23-45.
- [2] P.P. Sullivan, J.C. Weil, E.G. Patton, H.J.J. Jonker and D.V. Mironov 2016 *Turbulent winds and temperature fronts in large eddy simulations of the stable atmospheric boundary layer*, Journal of the Atmospheric Sciences **73**, 1815-1840.
- [3] R.J. Beare *et al.* 2006 *An intercomparison of large-eddy simulations of the stable boundary layer*, Boundary-Layer Meteorology **118**, 242-272.
- [4] D. Chung and G. Matheou 2012 *Direct numerical simulation of stationary homogeneous stratified sheared turbulence*, Journal of Fluid Mechanics, **696**, 434-467.
- [5] T. Gerz, J. Howell and L. Mahrt 1994 *Vortex structures and microfronts*, Physics of Fluids, **6**, 1242-1251.
- [6] Z. Warhaft 2000 *Passive scalars in turbulent flows*, Annual Review of Fluid Mechanics, **32**, 203-240.
- [7] R.J. Adrian 1996 *Stochastic estimation of the structure of turbulent fields*, in Eddy Structure Identification, J.P. Bonnet, Ed., Springer Verlag, 145 – 196.
- [8] J. Zhou, R. J. Adrian, S. Balachandar and T. M. Kendall 1999 *Mechanisms for generating coherent packets of hairpin vortices in channel flow*, Journal of Fluid Mechanics, **387**, 353-396.
- [9] R. J. Adrian 2007 *Hairpin vortex organization in wall turbulence*, Physics of Fluids, **19**, 041301.

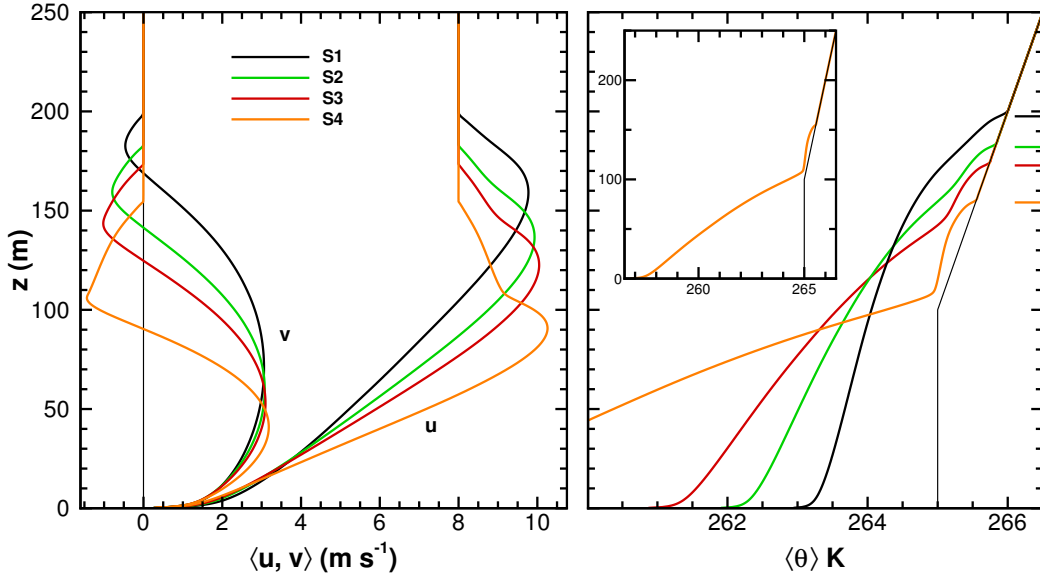


Figure 1: Vertical profiles of mean wind components  $\langle u, v \rangle$  (left panel) and mean temperature  $\langle \theta \rangle$  (right panel) in the stable atmospheric boundary layer for varying surface cooling rates  $C_r = (0.25, 0.375, 0.5, 1.0) \text{ K hr}^{-1}$  denoted by (black, green, red, orange) lines, respectively. The thin black line in the right panel is the initial temperature sounding and the horizontal lines along the right axis denote the boundary layer height.

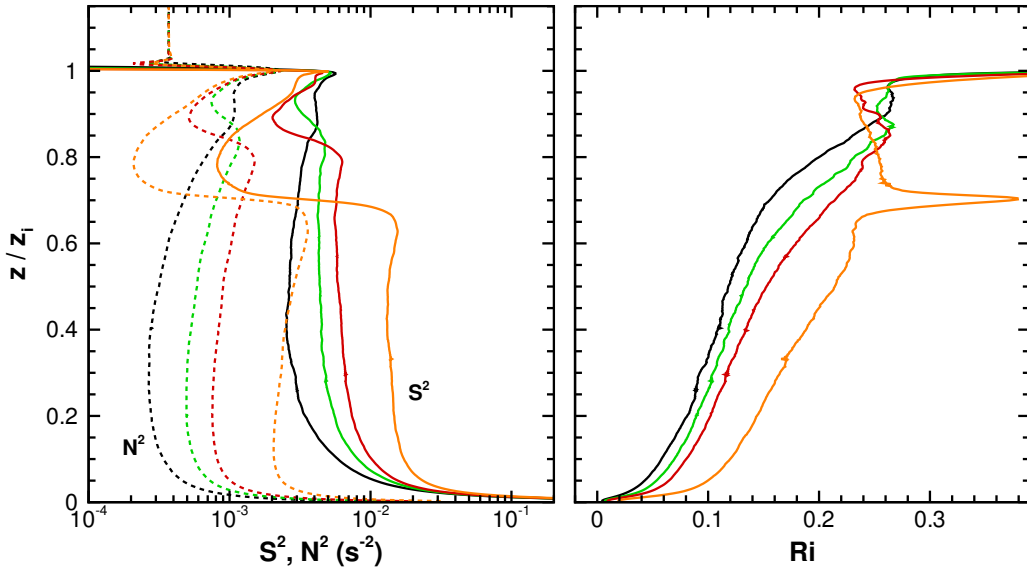


Figure 2: Vertical profiles of the average shear and buoyancy frequency squared ( $S^2, N^2$ ) (left panel) and gradient Richardson number  $Ri$  (right panel) for the same simulations as in Fig. 1. The (solid, dotted) lines in the left panel denote ( $S^2, N^2$ ), respectively. The mean gradients of velocity and temperature are used in the computation of ( $S^2, N^2, Ri$ ).

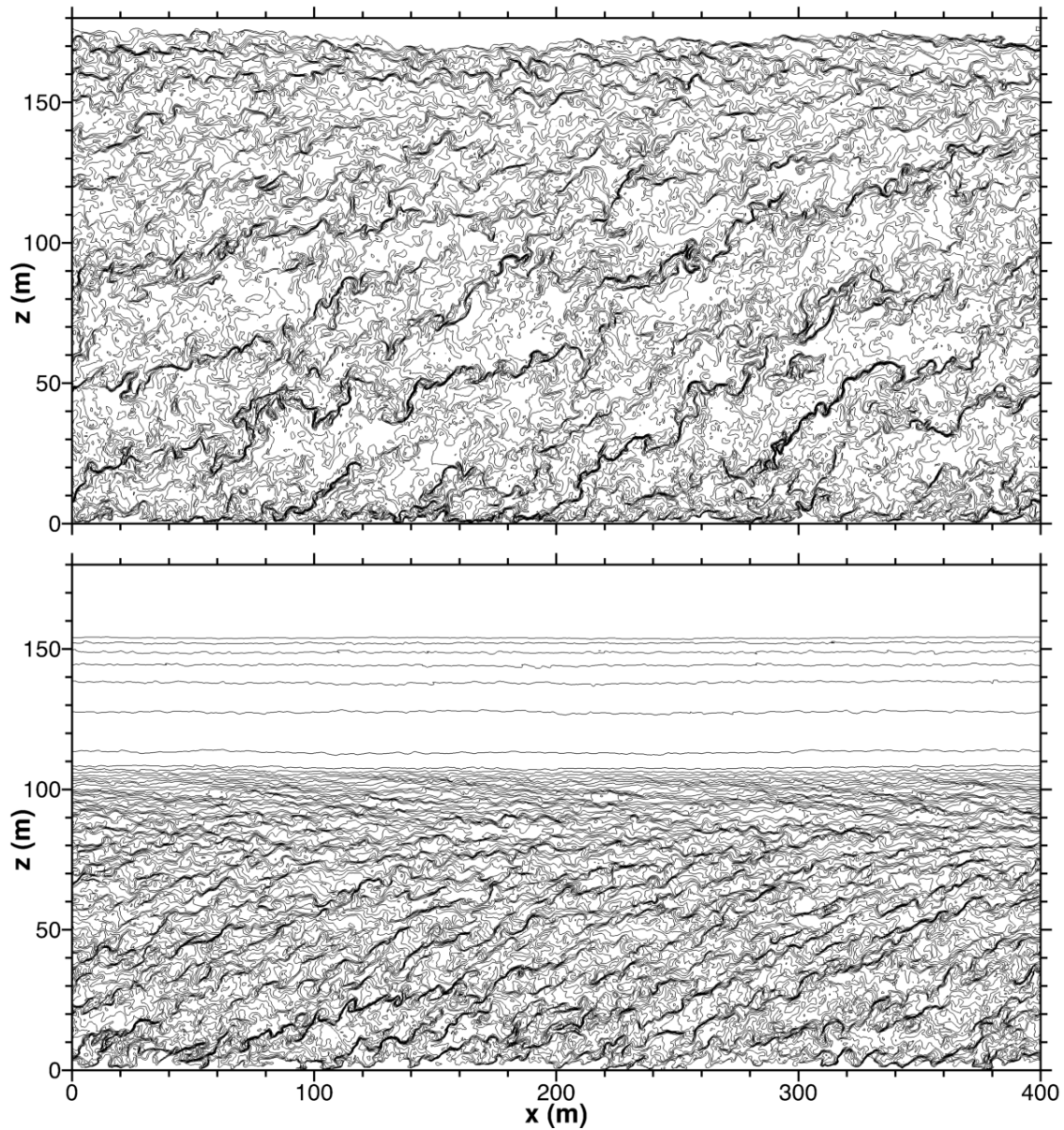


Figure 3: Contours of the temperature difference  $\theta - \theta_o$  in an  $x$ - $z$  plane from an LES of the nighttime stable boundary layer. Upper panel stratification  $z_i/L = 1.7$  with 71 equally spaced contour levels spanning the range  $[-2, 0]$  K. Lower panel stratification  $z_i/L = 6.0$  with 101 contour levels spanning the range  $[-8.0, 0.5]$  K. Notice how the tilt angle of the fronts is reduced with stronger stratification.

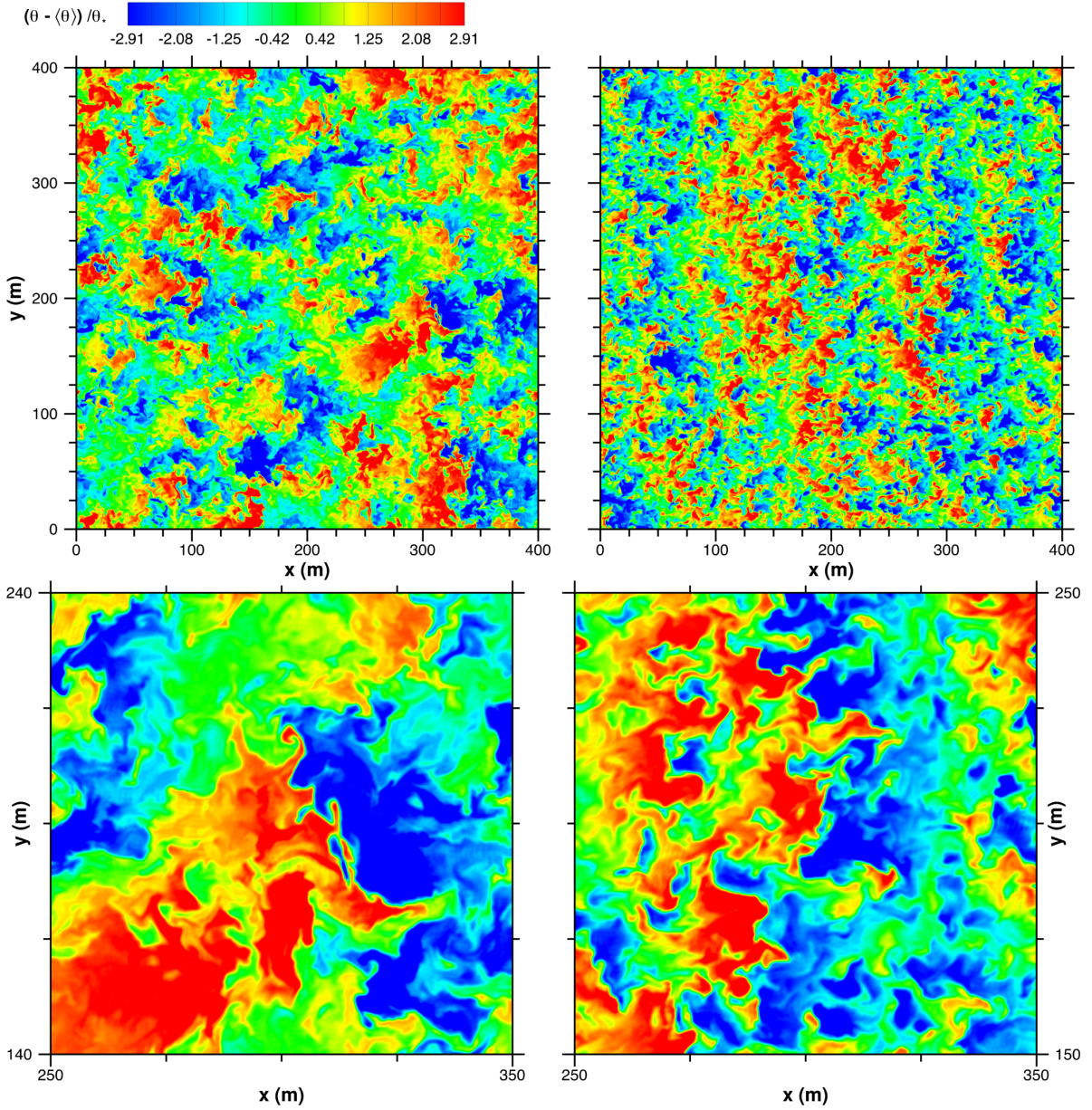


Figure 4: Contours of the non-dimensional temperature fluctuation  $\tilde{\theta}' = (\theta - \langle \theta \rangle) / \theta_*$  in an  $x$ - $y$  plane at  $z/z_i = 0.2$ . Weak surface cooling  $C_r = 0.25 \text{ K hr}^{-1}$  at  $z = 39.5 \text{ m}$  (left panels) and strong surface cooling  $C_r = 1.0 \text{ K hr}^{-1}$  at  $z = 30.8 \text{ m}$  (right panels). The zoomed images show the front detail over an area of  $100 \times 100 \text{ m}^2$ . Notice how the horizontal scale of the fronts decreases while the number of fronts increases with increasing stratification. The color bar is the same between all the images.

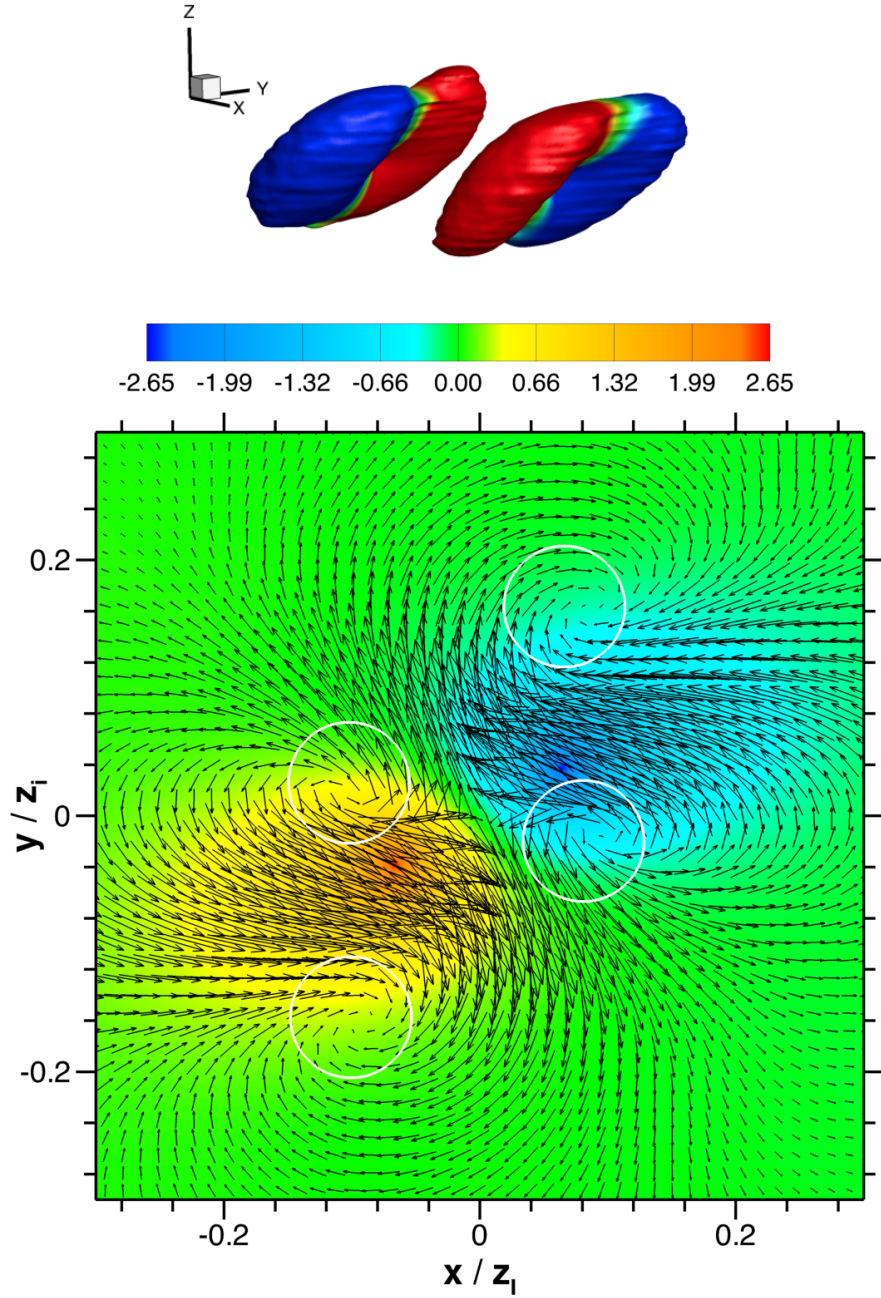


Figure 5: Upper image an oblique view of the vortical structures upstream and downstream of a temperature front from simulation S1 deduced using linear stochastic estimation. The isosurface shown corresponds to a low value of swirl [2,8], and is colored by the vertical component of the rotation vector  $\zeta \hat{\mathbf{z}}$  to indicate the sign of rotation. Deep (blue, red) colors indicate (negative-downward, positive-upward) rotation. The lower image is a horizontal  $x - y$  cut through the vortical structures in the upper image. The perturbation flow vectors  $(\hat{u}, \hat{v})$  overlay color contours of the perturbation temperature  $\hat{\theta}$  normalized by  $\theta_*$ . The white circles indicate the approximate location of the vortical legs in the upper image. The number of flow vectors is decimated by a factor of 7 in each direction compared to the grid resolution. Notice the sharp rotated temperature front that develops between the vortices.

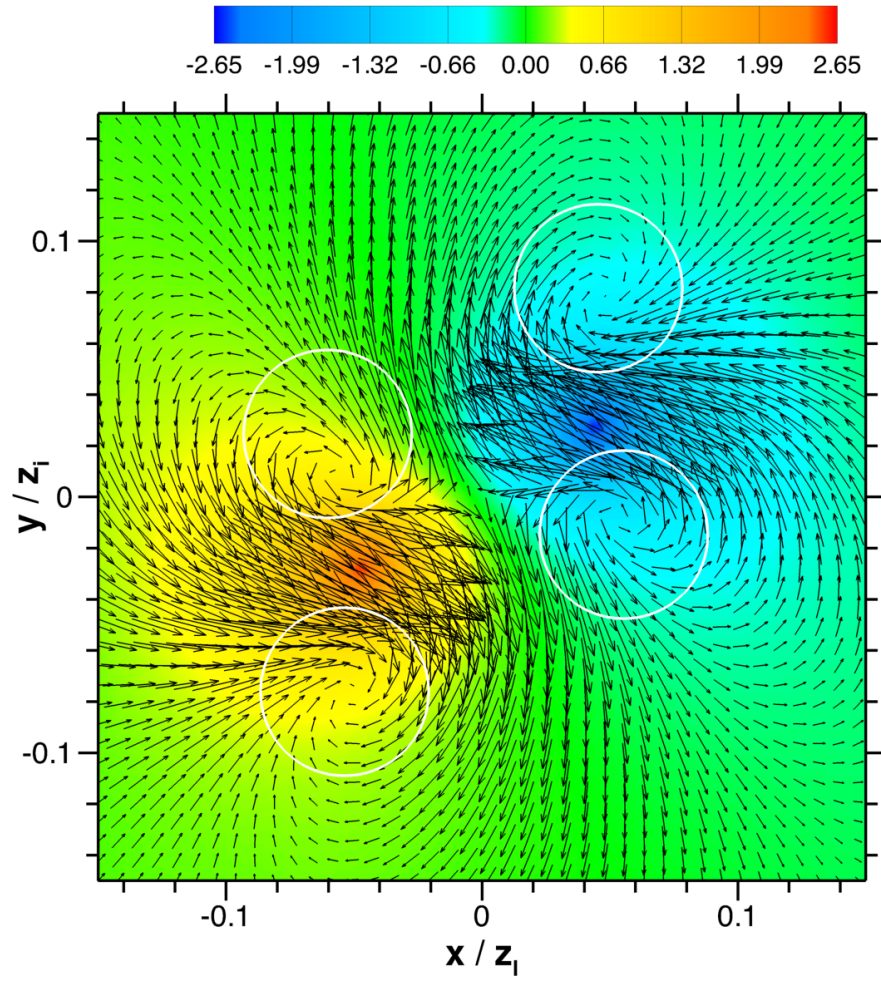


Figure 6: *Perturbation flow vectors and normalized perturbation temperature from simulation S4 with four times stronger surface cooling than S1. The labeling is identical to Fig. 5 except the horizontal dimensions are reduced.*